CHAPTER IV

EFFECTS OF HUMAN BODY ON WEARABLE ANTENNA

4.1 INTRODUCTION

In principle, components of WBAN operate in proximity to a human body although WBAN devices are typically wrist-worn to facilitate their accessibility and augment to the comfort of the wearer [1]. A current trends survey revealed that highest share of the wearable product market is dominated by wrist-worn wearable devices (approximately 35% of the market share), thus opening possibilities for numerous applications of wrist-based antennas [2]. A human wrist, consists of layers of - skin, fat, blood, nerve, muscle, and bone all of which have different dielectric properties [3]. The dimensions of the wrist vary from person to person and the performance of the wrist-worn device may vary accordingly. Hence, it is important to study the antenna characteristics vide S_{11}, bandwidth, radiation pattern and gain with respect to variation in human wrist parameters. Moreover, the orthogonal fields in rectangular patch antenna might be affected in dissimilar way when bent over the wrist along the two orthogonal bending planes and thus requires analysis.

The groove incorporated flexible antenna with self-compensating mechanism developed in Chapter III has been adopted for the studying over human wrist in the current chapter. The human body effects on the antenna performance are mostly studied using electromagnetic (EM) phantoms. These body phantoms are categorized as theoretical phantom and the voxel phantom (realistic model), which essentially employs simulated biological tissue and the actual physical structure, respectively [4, 5, 6]. Herein, a physical phantom is developed in-lab and the flexible antenna performance is tested on the phantom. The performance of the antenna worn on the wrist phantom is analysed in terms of gain, directivity and -10 dB bandwidth. A simulation study is also carried out employing a numerical phantom and electric field analysis is conducted to gain an insight of the results. Notably, most of the studies of human hand effect on the antenna, have resorted to use of phantom models of fixed dimension. However, in an adult human, wrist median radius ranges from 40mm to 20mm [7, 8, 9] and this will have effect on the antenna performance. In the current work, phantoms

of radii 40mm, 30mm and 20mm are used for analysing its effect on the antenna's performance.

4.2 SIMULATION STUDY

A human hand/wrist phantom is considered as a six-layered model from top skin layer down to the bone as core layer. Alkhamis et. al demonstrated a six layered numerical hand phantom to evaluate the effects on a 'wristband' antenna [3]. They reported mass density of the six tissues viz., skin, fat, nerve, blood, muscle, and bone for a thickness of 40 mm hand radius. In the current work, a 30mm and 20mm hand phantom is also considered for the study by remodelling the thickness parameter proportionately. Mass density and thickness variation for different hand radii is tabulated in Table 4.1.

Table 4.1 Mass density and thickness of the layers of the numerical human hand phantom

Tissue Name	Density (kg/m^3)	Thickness (mm) for 40mm hand radius *	Thickness (mm) for 30mm hand radius	Thickness (mm) for 20mm hand radius
Skin (dry)	1109	1.5	1.125	0.75
Fat	911	1.5	1.125	0.75
Nerve	1075	1	0.75	0.5
Blood	1050	4	3	2
Muscle	1090	15	11.25	7.5
Bone Marrow	1908	17	12.75	8.5

*Values as obtained from [3]

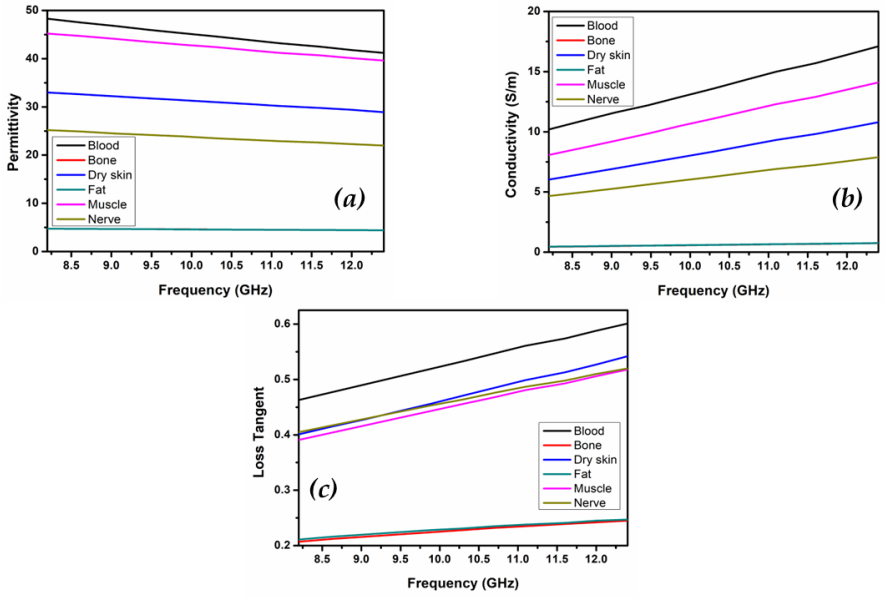

Figure 4.1 (a) Permittivity, (b) conductivity and (c) loss tangent values of the human tissues in X-band (8.2–12.4 GHz) as obtained from database [10]

The dielectric properties of the different tissues of the six-layered model, are taken from an open-source website [10]. The permittivity, loss tangent and conductivity values, as reported, has been plotted in the X-band range as shown in Figure 4.1(a-c).

The simulated hand phantom is modelled in CST Microwave Studio and represented schematically in Figure 4.2 using the dielectric parameters from plots in Figure 4.1 and thickness profile from Table 4.1. The simulation is carried out for both the bending topologies.

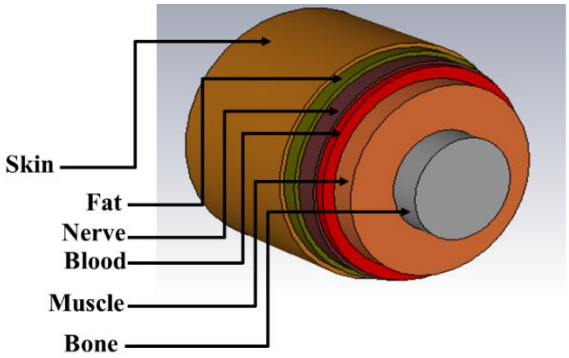

Figure 4.2 Six-layered human hand/wrist model

4.2.1 Topology I - XZ bending

The S_{11} plots for the Topology I antenna with varying hand phantom radii are shown in Figure 4.3. For reference, the corresponding S_{11} are plotted for the same antenna bent in free space (simulated as cylinders with air dielectric).

A marginal variation in the resonant frequencies of the antenna over hand phantom and over air is observed although there is no significant change in the -10 dB % bandwidth values of the corresponding configurations.

The radiation pattern of the Topology I antenna are shown in Figure 4.4 for XZ radiation plane and Figure 4.5 for YZ radiation plane.

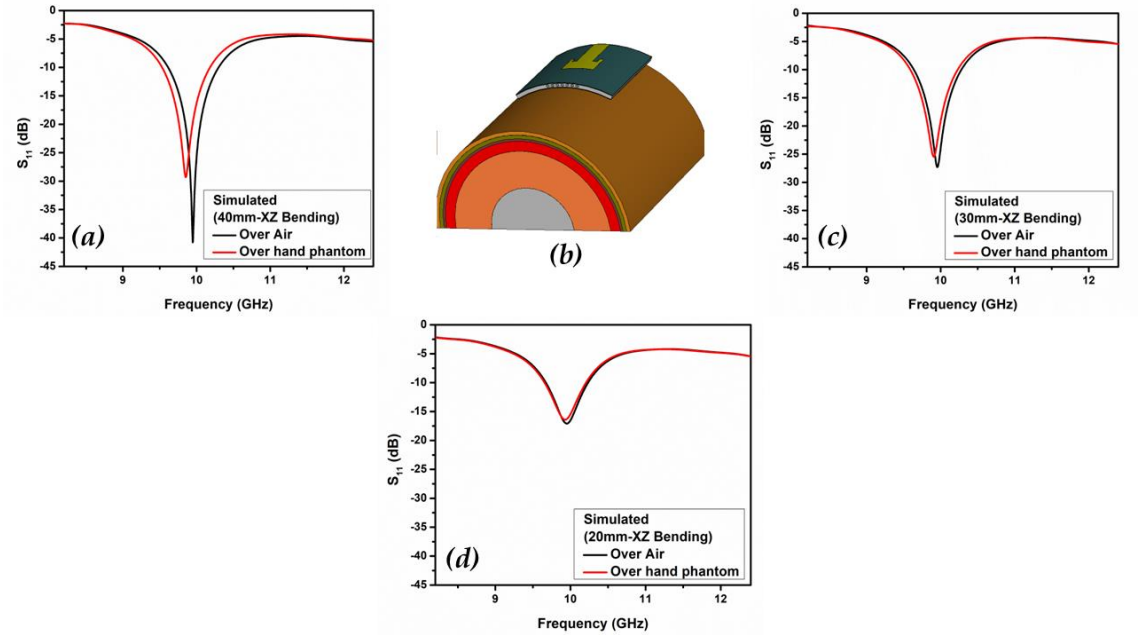

Figure 4.3 Simulated S_{11} plots of Topology I antenna for (a) 40mm radius, (b) schematic of the structure, (c) 30mm and (d) 20mm bending radius

As seen from Figure 4.3(b), the phantom is curtailed to a semi-cylinder instead of the full cylinder (refer Figure 4.2), primarily to reduce the computational size. This curtailment has been analysed and found to have no effect on the outcomes of the simulation.

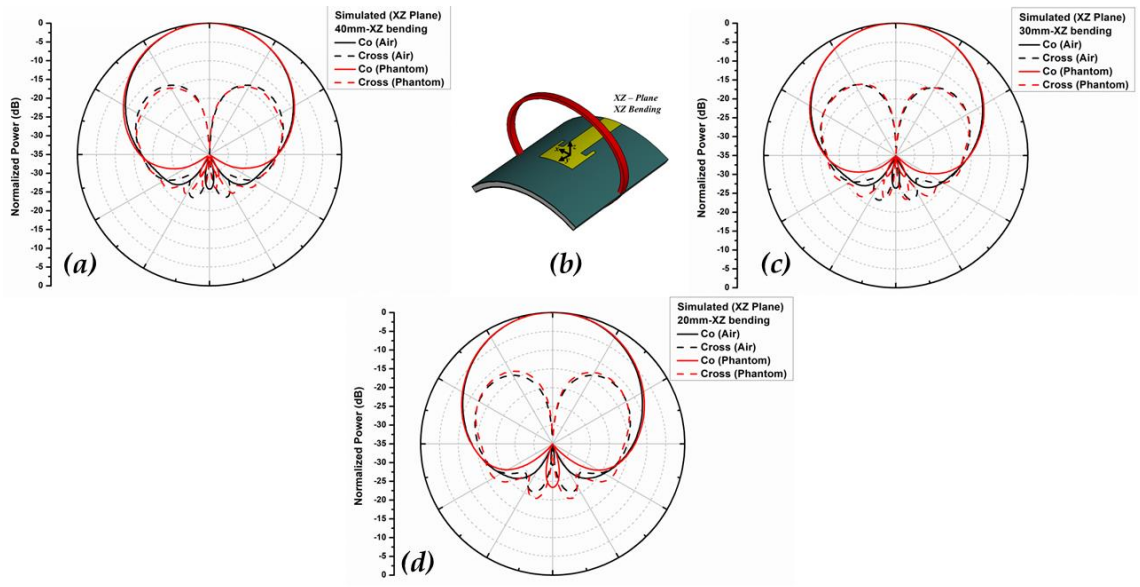

Figure 4.4 Simulated radiation pattern (XZ-plane) plots of Topology I antenna for (a) 40mm radius, (b) schematic illustration of bending and radiation plane, (c) 30mm and (d) 20mm bending radius

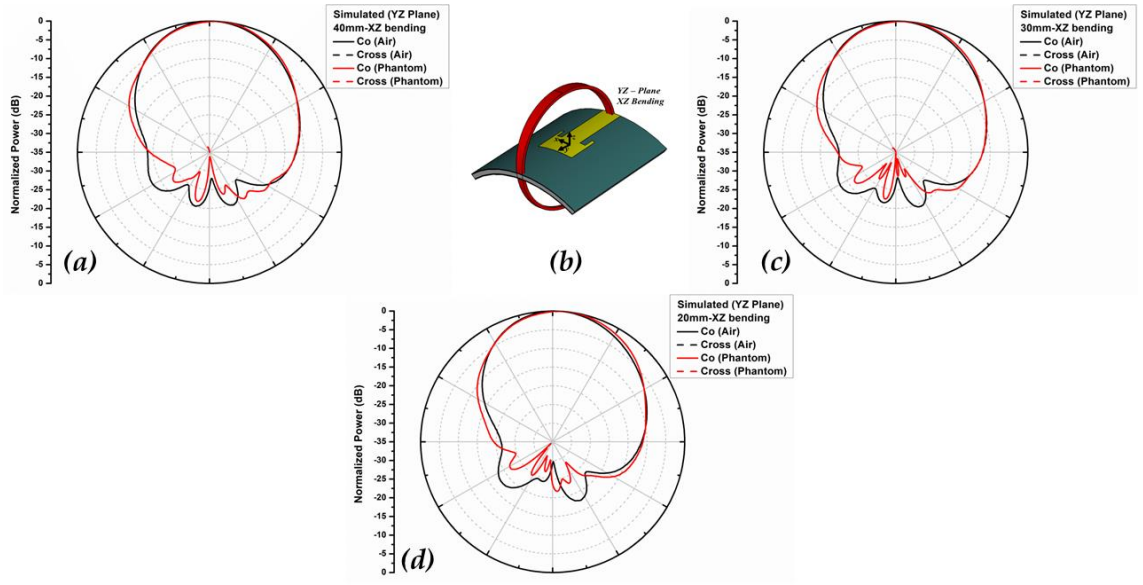

Figure 4.5 Simulated radiation pattern (YZ-plane) plots of Topology I antenna for (a) 40mm radius, (b) schematic illustration of bending and radiation plane, (c) 30mm and (d) 20mm bending radius

The broadside pattern is not affected much by the presence of the hand phantom, however the back lobe levels of the antenna over hand phantom decreases relatively due to possible absorption by the human tissues. The cross polar level of the antenna in YZ plane are much below the corresponding co-polar levels and hence the plots are not visible within the range as evident from Figure 4.5 (a, c and d).

4.2.2 Topology II - YZ bending

The S_{11} characteristics of the Topology II antenna, i.e., for YZ bending are shown in Figure 4.6. It is observed that the resonant frequencies and the -10 dB % bandwidth are hardly affected when the antenna is bent over the hand phantom in the YZ plane.

The radiation patterns of the Topology II antenna are shown in Figure 4.7 for XZ radiation plane and 4.8 for YZ radiation plane.

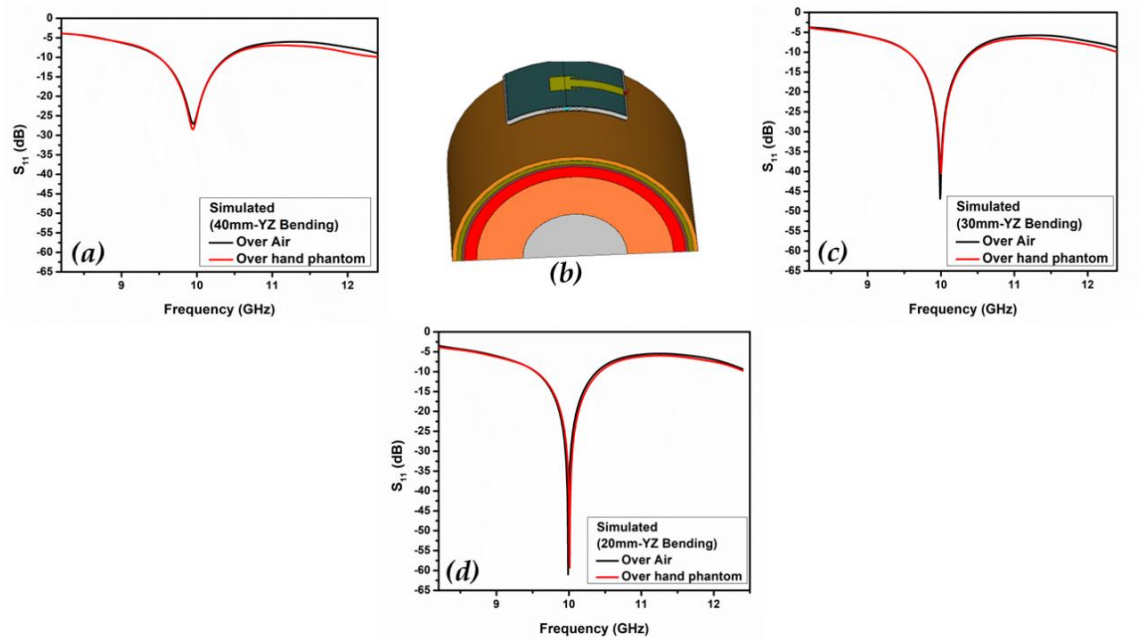

Figure 4.6 Simulated S_{11} plots of Topology II antenna for (a) 40mm radius, (b) schematic of the structure, (c) 30mm and (d) 20mm bending radius

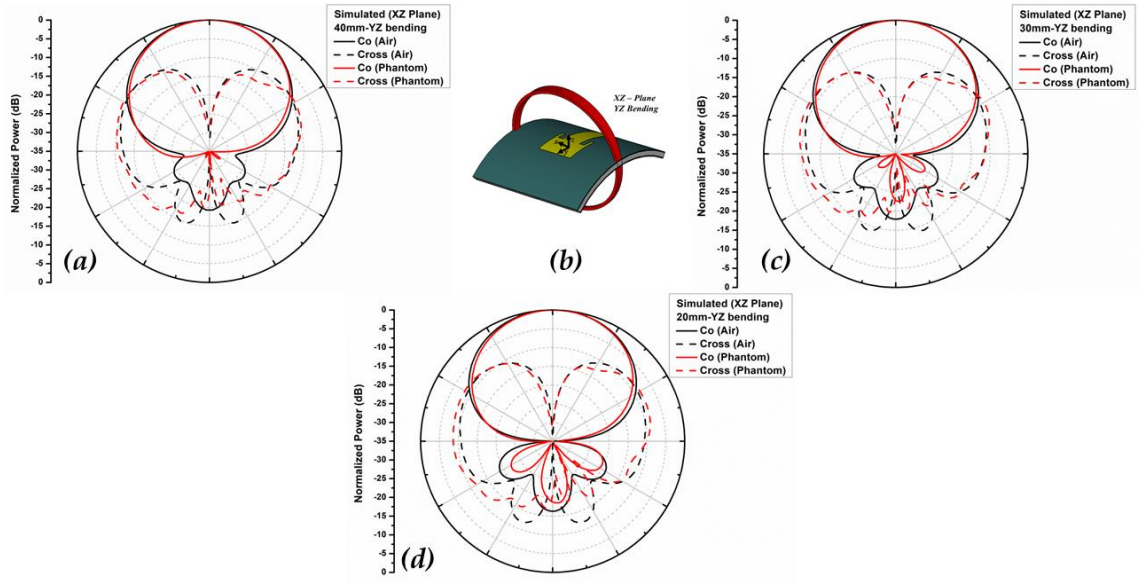

Figure 4.7 Simulated radiation pattern (XZ-plane) plots of Topology II antenna for (a) 40mm radius, (b) schematic illustration of bending and radiation plane, (c) 30mm and (d) 20mm bending radius

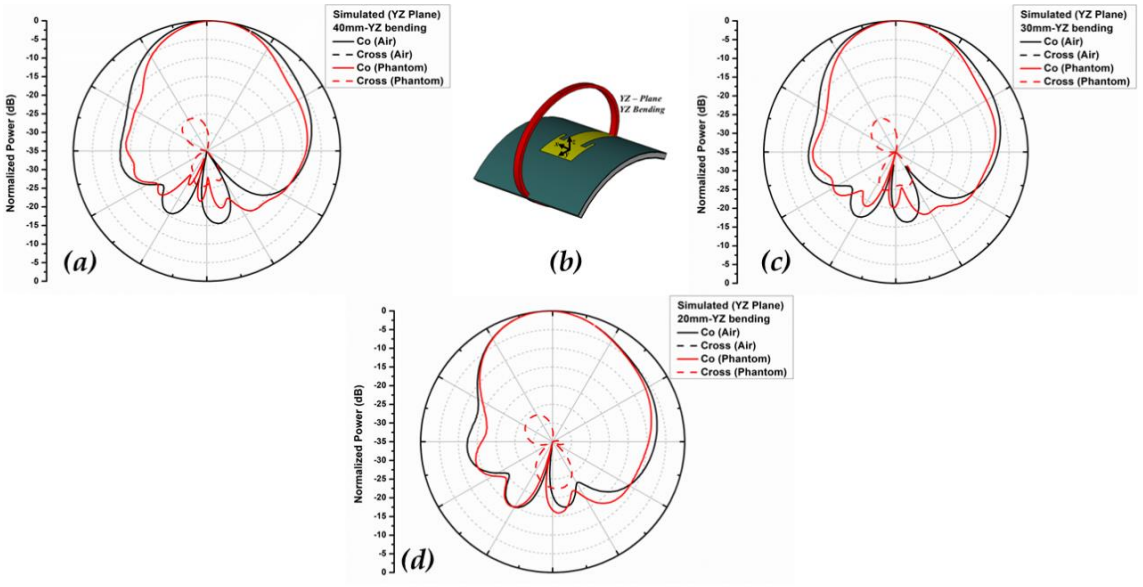

Figure 4.8 Simulated radiation pattern (YZ-plane) plots of Topology II antenna for (a) 40mm radius, (b) schematic illustration of bending and radiation plane, (c) 30mm and (d) 20mm bending radius

Herein also, the back lobe levels of the antenna over hand phantom decreases relatively as in case of XZ bending.

A summary of the obtained results from simulation is tabulated in Table 4.2.

Table 4.2 Summary of the results of the simulation study

Profile	*Bending Radii (mm)*	*Resonant Frequency (GHz)*	*S_{11} (dB)*	*-10 dB % BW*	*Directivity (dBi)*	*Gain (dBi)*	*Resonant Frequency (GHz)*	*S_{11} (dB)*	*-10 dB % BW*	*Directivity (dBi)*	*Gain (dBi)*
		Over Phantom					***Over Air***				
Topology I (XZ Bending)	***40***	*9.85*	*-29*	*6.7*	*9.1*	*7.5*	*9.94*	*-40*	*6.8*	*9.2*	*7.6*
	30	*9.90*	*-25*	*6.4*	*8.9*	*7.3*	*9.95*	*-27*	*6.4*	*9.1*	*7.6*
	20	*9.93*	*-16*	*5.5*	*8.5*	*7.0*	*9.95*	*-17*	*5.6*	*8.7*	*7.2*
Topology II (YZ Bending)	***40***	*9.94*	*-28*	*9.3*	*9.1*	*6.9*	*9.95*	*-27*	*9.1*	*8.1*	*6.1*
	30	*9.99*	*-40*	*9.1*	*8.8*	*6.6*	*9.98*	*-46*	*8.4*	*8.0*	*6.1*
	20	*10.01*	*-59*	*7.8*	*8.4*	*6.1*	*9.98*	*-60*	*8.5*	*8.0*	*6.0*

The trends in variation of antenna parameters for both the topologies and all bending profiles are experimentally verified.

4.3 EXPERIMENTAL STUDY

The effect of human hand on the antenna's performance is experimentally tested in two phases. In the first phase a realistic EM phantom is developed and tested for its microwave dielectric properties. In the second phase, the two differently grooved antennas viz., Topology I and Topology II are measured for their resonant and radiating characteristics over the developed human hand phantoms.

4.3.1 Development and dielectric characterization of realistic EM hand phantom

Realistic EM phantoms or Tissue Mimicking Materials (TMMs) are either liquid based [11], semi-solid gel type [12] or solid based [13]. The liquid-based phantoms are suitable for invasive measurements like SAR, though it poses certain restrictions in carrying out measurements involving rotation of the phantom, for e.g., in full spherical radiation measurements. Solid phantoms can overcome this issue as it can be well integrated with positioner turn tables to carry out measurement at any degree of inclination. Moreover, solid phantoms have a better shelf life than liquid phantoms.

Hand phantoms, or in general limb phantoms have been designed for a wide band of frequencies ranging from few kHz to tens of GHz and have been applied for hyperthermia studies as well as for wearable communication systems [14]. Gabriel et. al and Garrett et. al. had developed a human hand palm phantom using silicone-carbon composites and demonstrated its applicability in the frequency range 10 MHz to 10 GHz [15, 16].

Here, a solid-based hand phantom is developed to mimic the average dielectric properties of a human hand in the frequency range 8.2 GHz to 12.4 GHz. The phantom is developed using graphite powder (Make - Merck) mixed with silicone rubber (Make - Moldsil) in the weight ratio 1:1 (or 50% wt.). The slurry is initially mixed for 15 minutes to obtain a homogenous mixture and then a hardener in a weight ratio of 5% is added for the curing process. Just at the onset

of the curing process, the mixture is poured slowly to avoid formation of air bubbles, into PLA 3D printed moulds (BoxzY, USA) of required shape and dimension. The curing process is carried out at room temperature for 24 hours. After the mixture gets cured it hardens and takes the form of the mould.

Pellets of dimension (22.86 × 10.16) mm^2 of the same 50% graphite-silicone composite is moulded for carrying out microwave dielectric characterization in X-band through transmission–reflection method using Nicholson-Ross-Weir (NWR) technique as detailed in Section 2.5 of Chapter II in (illustrated in Figure 4.9).

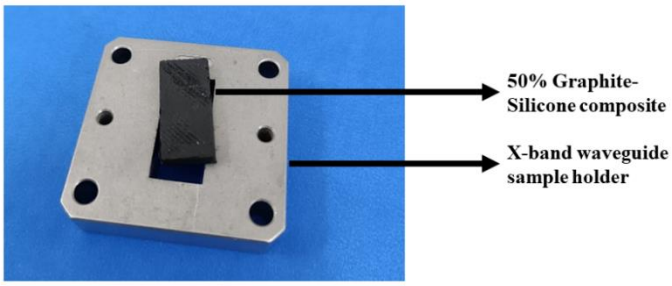

Figure 4.9 Fabricated graphite-silicone composite for microwave characterization

The obtained permittivity and loss tangent plots are in Figure 4.10(a) and 4.10(b) respectively.

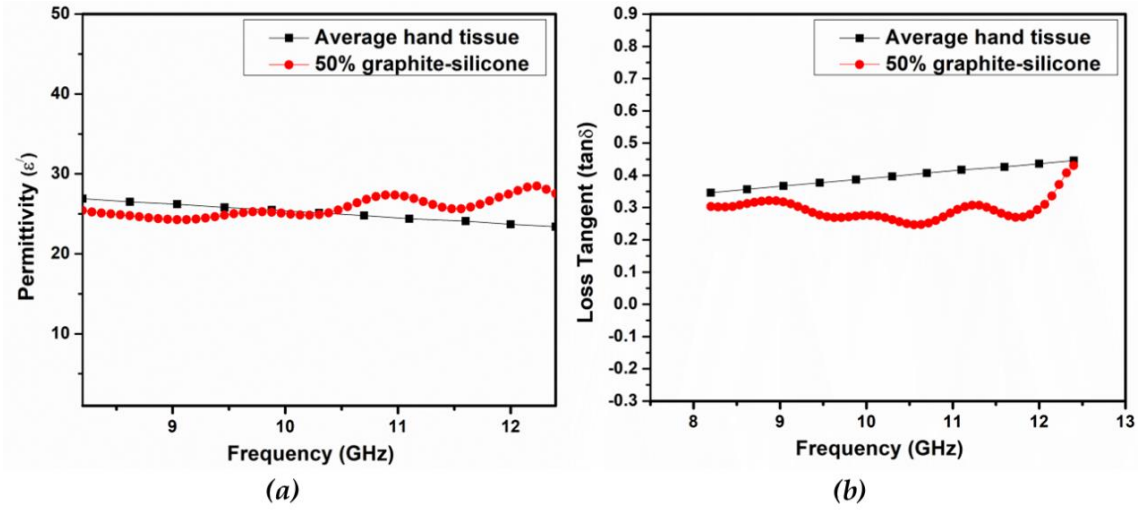

Figure 4.10 (a) Permittivity and (b) loss tangent of the fabricated 50% graphite-silicone composite compared to average dielectric value of hand tissue obtained from [10]

The results are compared with the average dielectric values of human hand available in an open-source website [10] and explicitly furnished in Table 4.3.

Table 4.3 Comparative chart of the permittivity and loss tangent values from Figure 4.10

Frequency (GHz)	**8.2**	**8.62**	**9.04**	**9.46**	**9.88**	**10.3**	**10.7**	**11.1**	**11.6**	**12**	**12.4**
ε′ (obtained from [9])	26.9	26.5	26.2	25.8	25.5	25.1	24.8	24.4	24.1	23.7	23.4
ε′ (developed phantom)	25.4	24.7	24.2	24.8	25.2	24.9	26.8	26.9	25.8	27.9	27.5
tanδ (obtained from [9])	0.34	0.35	0.36	0.37	0.38	0.39	0.40	0.41	0.43	0.43	0.44
tanδ (developed phantom)	0.30	0.31	0.31	0.27	0.27	0.26	0.25	0.30	0.27	0.30	0.43

The permittivity values of the developed composite and average dielectric values of the hand are in seamless agreement in the mid X-band range between 9.7-10.3 GHz, which is the working band of the current work and thus will be suitable for evaluating the effect on the wearable antenna's performance. The developed hand phantoms prototype of radius 40, 30 and 20mm as shown in Figure 4.11.

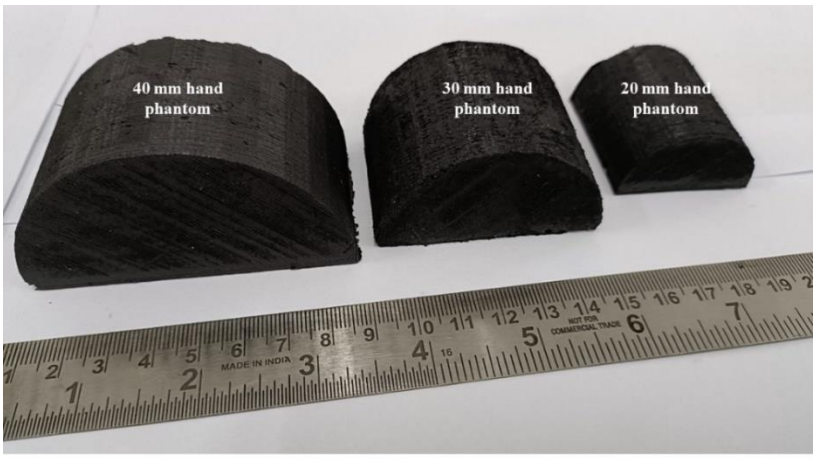

Figure 4.11 Developed human wrist/hand phantom of radii 40mm, 30mm and 20mm

4.3.2 Evaluation of antenna performance over EM phantom

Topology I

As described in the preceding section, in Topology I, bending is carried out in the XZ plane Figure 4.12(a). The S_{11} plots for the Topology I antenna placed on the hand phantom with varying radii are shown in Figures 4.12(b-d). For reference, the corresponding S_{11} are plotted for the same antenna bent in free space i.e., over PLA hollow semi cylinders.

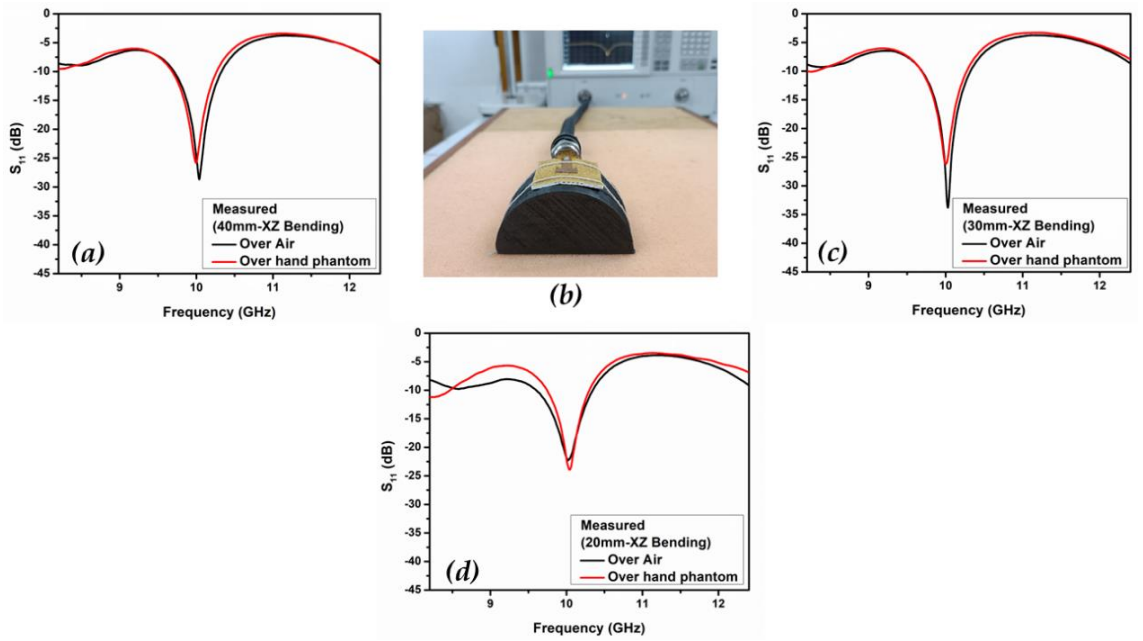

Figure 4.12 Measured S_{11} plots of Topology I antenna for (a) 40mm radius, (b) photograph of antenna over 40mm phantom, (c) 30mm and (d) 20mm bending radius

The radiation patterns of the antenna over hand and over air for two orthogonal planes XZ and YZ are plotted in Figures 4.13 and 4.14 respectively.

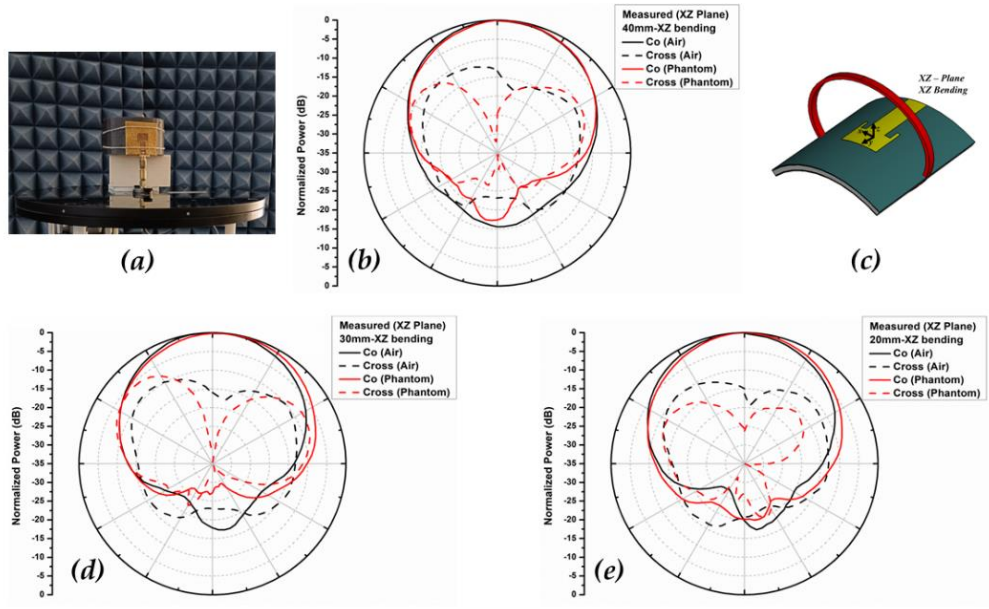

Figure 4.13 (a) Photograph of antenna on phantom for radiation pattern measurement, measured radiation pattern (XZ plane) plots of Topology I antenna for, (b) 40mm bending radius, (c) schematic illustration of bending and radiation plane, (d) 30mm and (e) 20mm bending radius

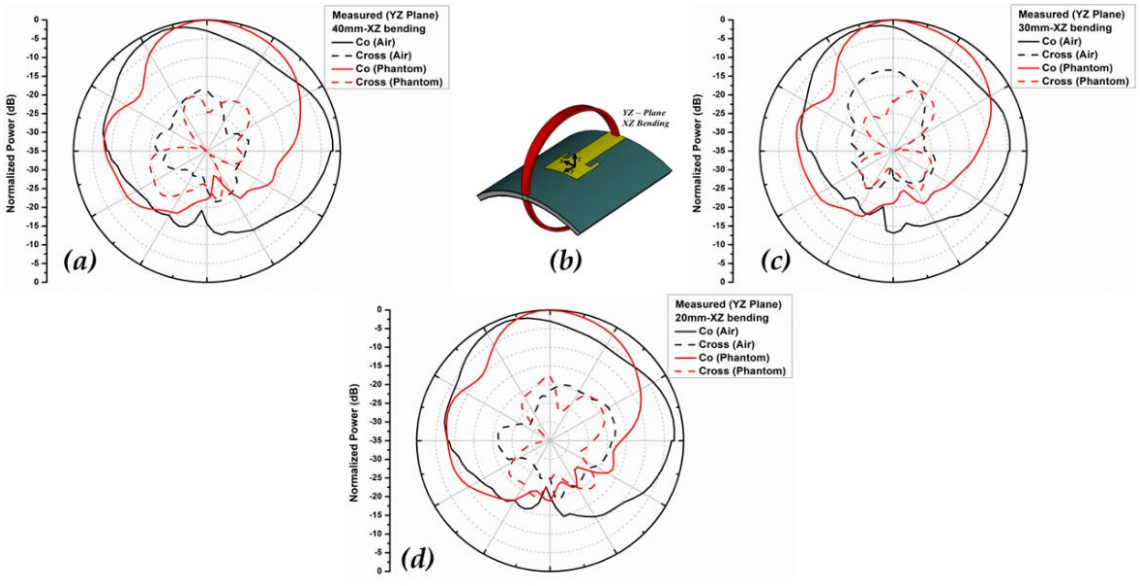

Figure 4.14 Measured radiation pattern (YZ plane) plots of Topology I antenna for (a) 40mm bending radius, (b) illustration of bending and radiation plane, (c) 30mm and (d) 20mm bending radius

Topology II

Topology II antenna is for the YZ bending and the S_{11} curves of the antenna over the hand phantom are plotted in Figures 4.15(a-c) along with the S_{11} curves for the same antenna bent in free space (over PLA hollow semi cylinders) for reference.

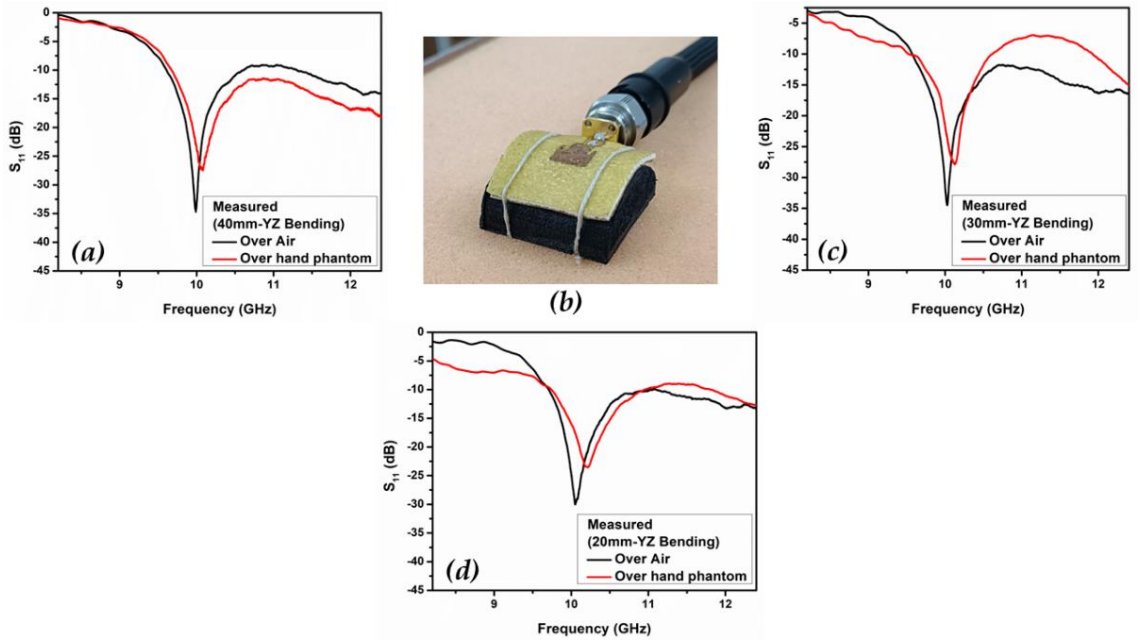

Figure 4.15 Measured S_{11} plots of Topology II antenna for (a) 40mm bending radius, (b) photograph of antenna over 40mm phantom, (c) 30mm and (d) 20mm bending radius

The corresponding radiation patterns in XZ and YZ planes are shown in Figure 4.16 and 4.17 respectively.

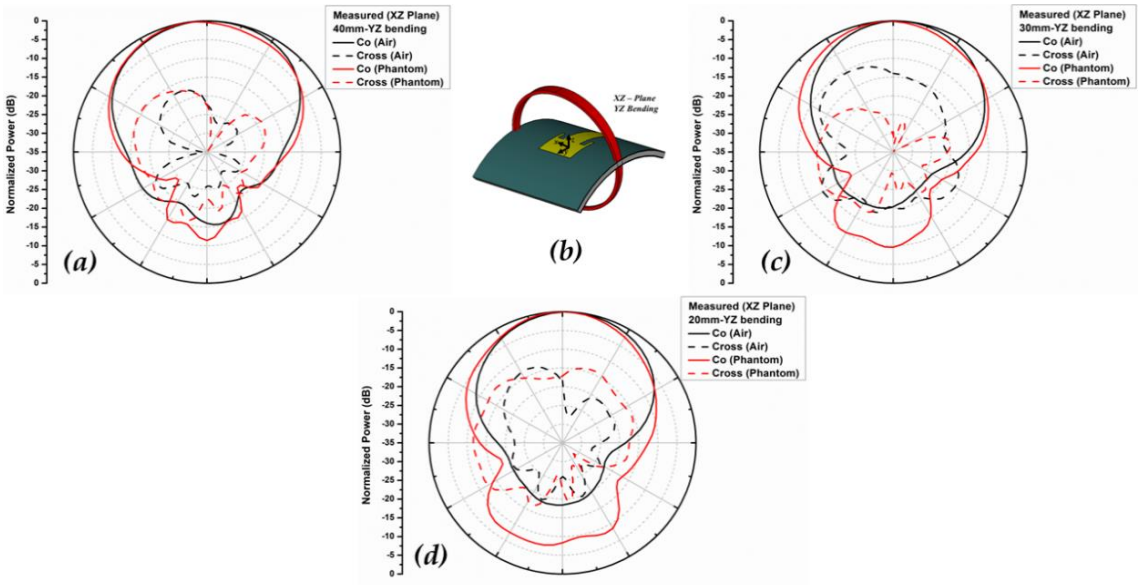

Figure 4.16 Measured radiation pattern (XZ plane) plots of Topology II antenna for (a) 40mm bending radius, (b) schematic illustration of bending and radiation plane, (c) 30mm and (d) 20mm bending radius

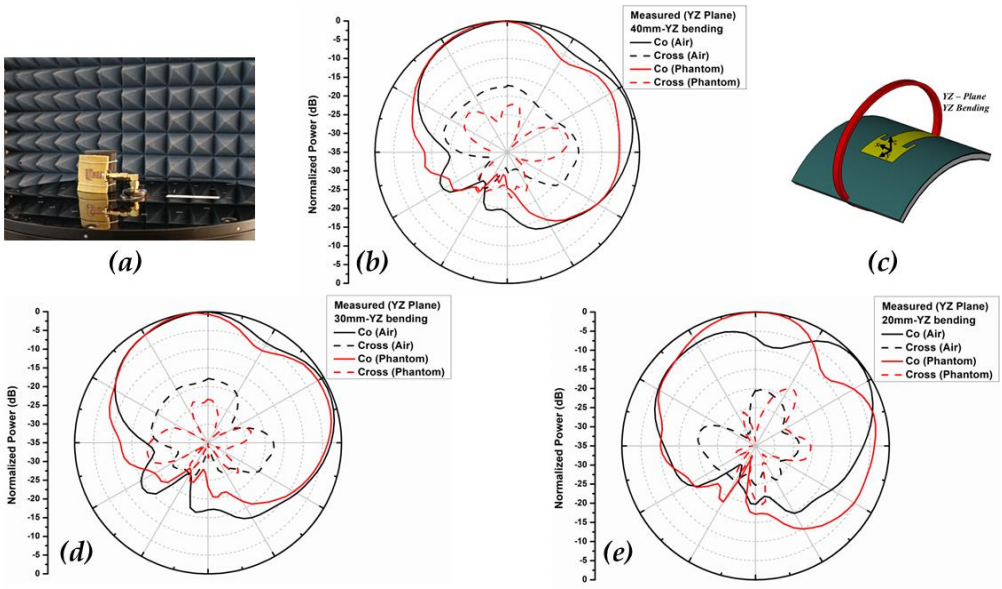

Figure 4.17 (a) Photograph of antenna on phantom for radiation pattern measurement, measured radiation pattern (YZ plane) plots of Topology II antenna for, (b) 40mm, (c) schematic illustration of bending and radiation plane, (d) 30mm and (e) 20mm bending radius

The summary of the experimental results is tabulated in Table 4.4.

Table 4.4 Summary of the results of the experimental study

Profile	*Bending Radii (mm)*	*Resonant Frequency (GHz)*	*S_{11} (dB)*	*-10 dB % BW*	*Directivity (dBi)*	*Gain (dBi)*	*Resonant Frequency (GHz)*	*S_{11} (dB)*	*-10 dB % BW*	*Directivity (dBi)*	*Gain (dBi)*
		Over Phantom					***Over Air***				
Topology I	***40***	*9.99*	*-25*	*5.7*	*9.8*	*7.9*	*10.03*	*-28*	*6.2*	*11.3*	*8.1*
(XZ	***30***	*10.00*	*-26*	*5.8*	*8.9*	*7.4*	*10.02*	*-33*	*6.3*	*11.3*	*7.9*
Bending)	***20***	*10.04*	*-23*	*5.5*	*9.2*	*7.1*	*10.01*	*-22*	*7.4*	*11.1*	*7.8*
Topology II	***40***	*10.08*	*-27*	*10.7*	*10.0*	*7.1*	*9.98*	*-34*	*10.1*	*10.2*	*7.0*
(YZ	***30***	*10.12*	*-27*	*10.8*	*10.4*	*7.0*	*10.02*	*-34*	*11.4*	*9.9*	*6.8*
Bending)	***20***	*10.21*	*-23*	*12.7*	*9.2*	*6.6*	*10.05*	*-30*	*13.2*	*8.1*	*6.7*

In case of Topology I i.e., XZ bending, the antenna's resonant frequency is slightly lower than the corresponding antenna bent on air. While for Topology II, i.e., YZ bending the resonance takes place at a marginal higher frequency as compared to its air counterpart. The S_{11} values for all the configurations (in dB) are less negative for the antenna over hand as compared to antenna over air. The directivity and gain values are reduced which indicates a reduction in radiation efficiency when placed over hand in the Topology I configuration, however, the values increase when the antenna is bent in the YZ plane when placed over the phantom. These trends are similar to the trends observed in the simulated results, refer Table 4.4.

4.4 ANALYSIS AND DISCUSSION

The impedance of the antenna is usually affected when any object having high permittivity or conductivity is placed in its near field region of the antenna [17]. The reactive near field region of an antenna R_{NF} is given by $R_{NF} \leq 0.62\sqrt{D^3/\lambda}$, where D is the largest aperture of an antenna [18]. The R_{NF} of the antennas considered in the study is calculated to be ≈ 28 mm. As in the current work the antenna is placed in direct contact with the human hand, the impedance will inevitably be affected. Along the length of the patch, the impedance variation is proportional to the electric field, with its value being zero at the centre of the patch and maximum at the edges [19]. The variation in impedance can be envisaged by analysing electric field distribution of the antenna in presence of the human hand along the length of the patch at the resonant frequencies. An along-

side field analysis is also carried out for antenna over air for both the topologies. The electric field distribution Topology I is illustrated in Figure 4.18(b-g) for all the profiles.

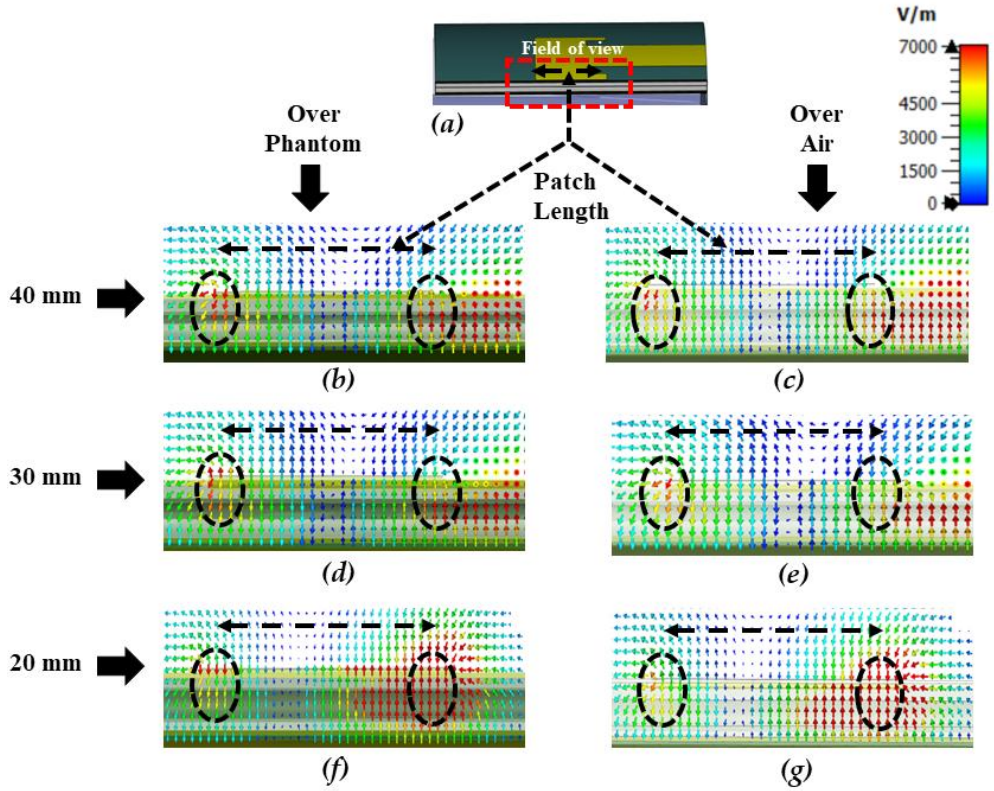

Figure 4.18 Simulated electric field distribution of Topology I antenna along the length of the patch (a) field of view, (b) over 40mm hand, (c) 40mm air, (d) over 30mm hand, (e) 30mm air, (f) over 20mm hand and (g) 20mm air

The electric field Figure 4.18(b, d, f) intensifies at the radiation edges when placed over phantom. This implies that the edge impedance of the antenna increases as compared to that placed on air.

Figure 4.19(b-g) are the field distribution of the Topology II antenna. In this case, the field intensity at the radiation edges is lowered over human hand as compared to over air, which indicates lowering of edge impedance.

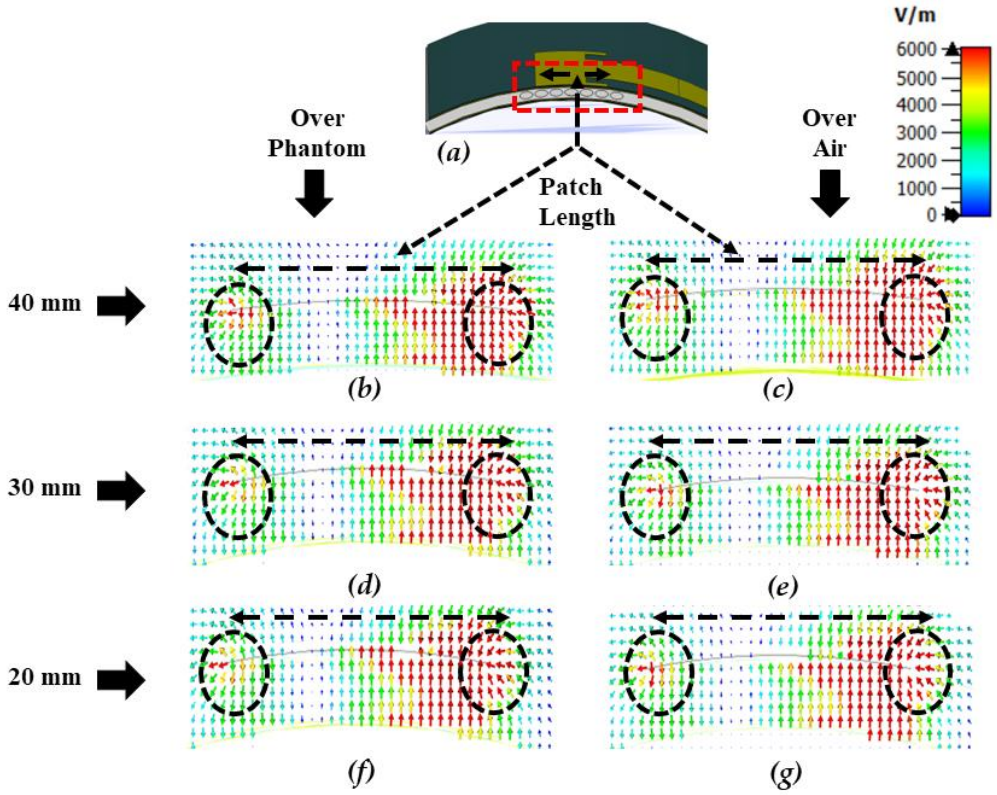

Figure 4.19 Simulated electric field distribution of Topology II antenna along the length of the patch (a) field of view, (b) over 40mm hand, (c) 40mm air, (d) over 30mm hand, (e) 30mm air, (f) over 20mm hand and (g) 20mm air

The impedance variation of the antenna over phantom with respect to air for the two bending directions is taking place in the opposite course. This would impact the fringing fields and consequently the electrical length of the patch [19]. Thus, the variation in the impedance observed can possibly be one of the factors leading to the frequency shift observed.

In on-body placements, the human body back-scatters energy changing induced current on the antenna structure [20]. Presence of co-phase current leads to increase in gain of the antenna, whereas cross-phase current decreases the gain [21]. Thus, the radiation pattern of a patch antenna can be correlated to its surface current distribution. The surface current variation on the patch of the Topology I on hand phantom of radii 40mm, 30mm and 20mm and the current distribution for the same bending on air is also shown alongside in Figure 4.20(a-f).

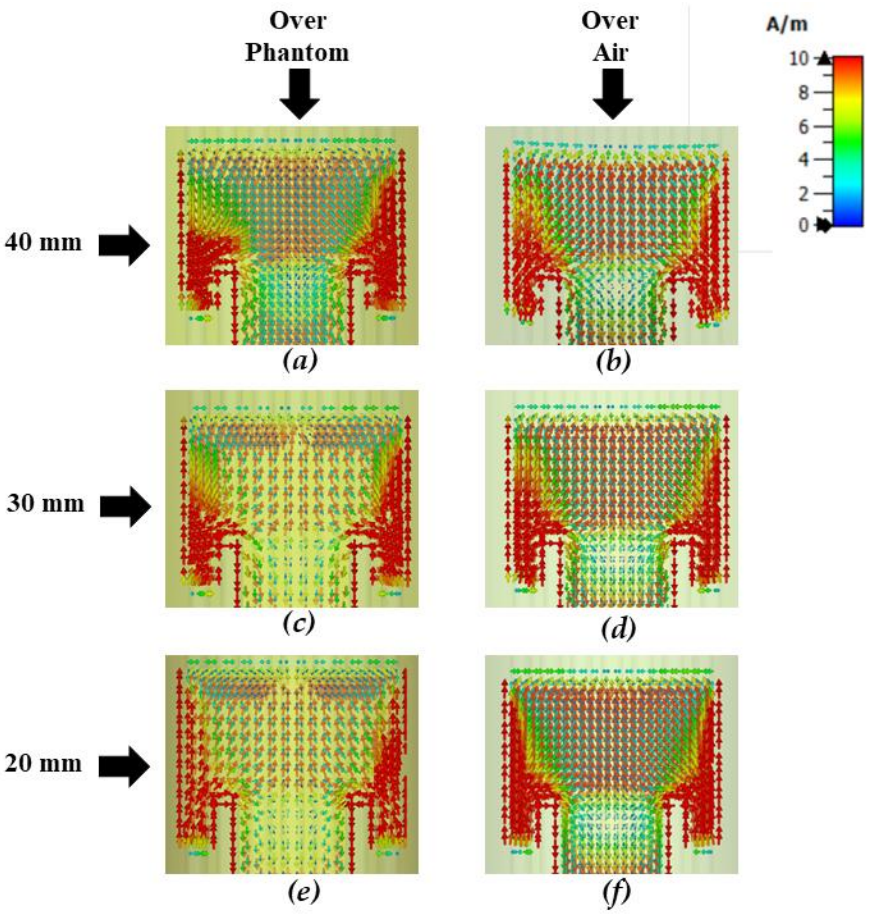

Figure 4.20 Simulated surface current distribution of Topology I antenna from the top view of the patch (a) over 40mm hand, (b) 40mm air, (c) over 30mm hand, (d) 30mm air, (e) over 20mm hand and (f) 20mm air

The current distribution for the antenna on the hand phantom is perturbed and asymmetrical with respect to the corresponding antenna on air. Moreover, the density of the current decreases as the antenna's bending radius is decreased. This could possibly lead to degradation of radiation pattern.

Figure 4.21(a-f) are the current distribution for Topology II antenna. Herein, the current distribution is denser for the patch over the hand, possibly leading to enhancement of gain.

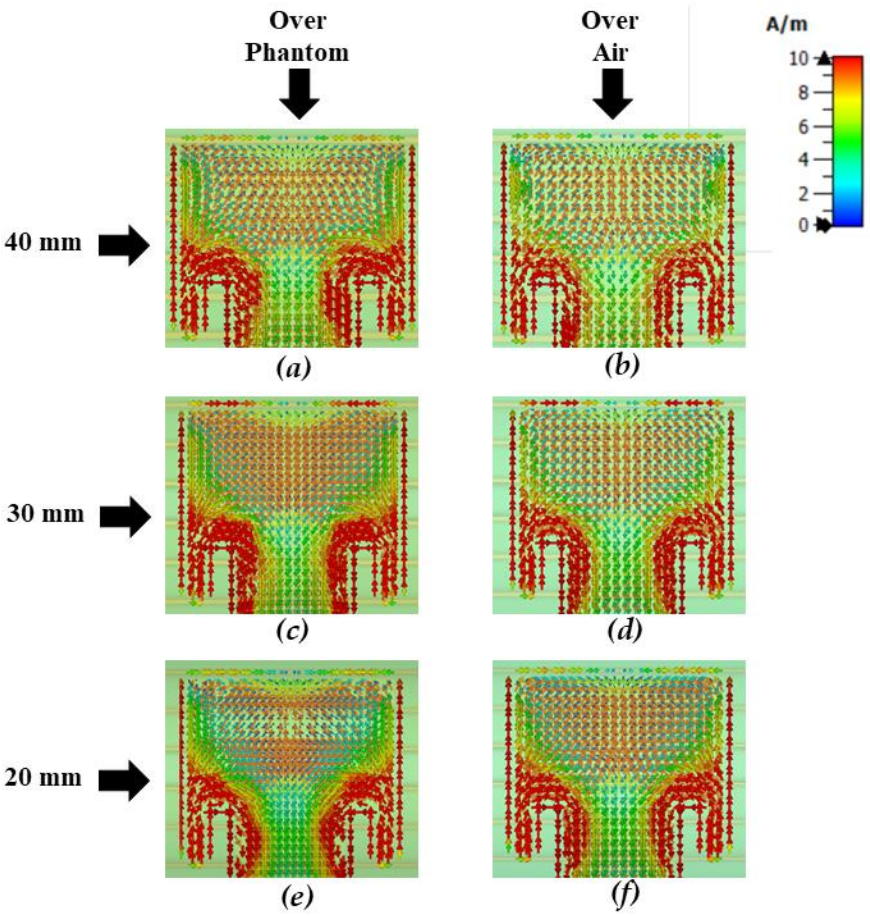

Figure 4.21 Simulated surface current distribution of Topology II antenna from the top view of the patch (a) over 40mm hand, (b) 40mm air, (c) over 30mm hand, (d) 30mm air, (e) over 20mm hand and (f) 20mm air

Referring to Figure 4.18, a higher field concentration is observed in beneath the patch in Topology I profiles when positioned over phantom, leading to a degradation of radiation efficiency while in Topology II profiles a reverse trend in distribution is seen, Figure 4.19.

A plot of the peak surface current density of all the configurations considered in the study is shown in Figure 4.22. The gain values of the antenna configurations (Table 4.4) follow a similar trend.

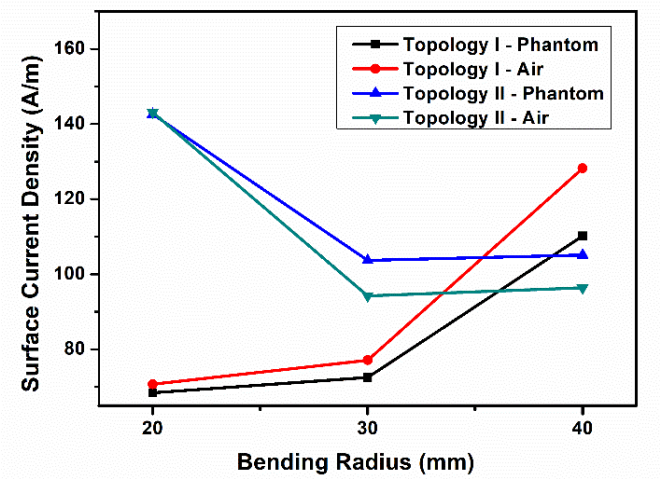

Figure 4.22 Peak surface current density (simulated) vs bending radius plot

4.5 SUMMARY

The performance study of a WBAN antenna based on silicone-polyurethane foam grooved substrate is conducted to analyse the effect on its parameters in presence of a human body. A six-layered simulated wrist/hand phantom is modelled for full wave simulation and a homogenous graphite-silicone phantom is developed for the experimental studies in the X-band regime. The said antenna is tested on phantoms of 40mm, 30mm and 20mm radii along two orthogonal bending planes. The resonant frequencies were marginally detuned with a maximum of ~1.5% when compared to the same antenna tested in free space. The antenna exhibited measured gain values of more than 6.6 dBi in all the bending configurations over the human phantom which is marginally less than that of the corresponding bending over air. The electric field and surface current analysis carried out provided an insight into the perturbations that occur due to the presence of the human phantom and due to the change in the size of the phantom which led to the variation in the performance as observed from the experimental study.

References

1. Al-Eidan, R.M., Al-Khalifa, H. and Al-Salman, A.M. A review of wrist-worn wearable: sensors, models, and challenges. *Journal of Sensors*, 1-20, 2018.
2. Berglund, M. E., Duvall, J., and Dunne, L. E. A survey of the historical scope and current trends of wearable technology applications. In *Proceedings of the 2016 ACM international symposium on wearable computers*, pages: 40-43, September 2016, ACM.
3. Alkhamis, R., Wigle, J. and Song, H. Global positioning system and distress signal frequency wrist wearable dual-band antenna. *Microwave and Optical Technology Letters*, *59*(8):2057-2064, 2017.
4. Nikolovski, M. Detailed Modeling of the Human Body in Motion to Investigate the Electromagnetic Influence of Fields in a Realistic Environment. Master's thesis, Technische Universität Darmstadt, 2018.
5. Muramatsu, D. and Sasaki, K. Transmission analysis in human body communication for head-mounted wearable devices. *Electronics*, *10*(10):1213, 2021.
6. Mahmood, S.N., Ishak, A.J., Saeidi, T., Soh, A.C., Jalal, A., Imran, M.A. and Abbasi, Q.H. Full ground ultra-wideband wearable textile antenna for breast cancer and wireless body area network applications. *Micromachines*, *12*(3):322, 2021.
7. Mousapour, P., Barzin, M., Valizadeh, M., Mahdavi, M., Hadaegh, F., Azizi, F. and Hosseinpanah, F. Wrist circumference as a novel predictor of transition from metabolically healthy to unhealthy phenotype in overweight/obese adults: a gender-stratified 15.5-year follow-up. *BMC Public Health*, *21*(1):1-10, 2021.
8. Jahangiri Noudeh, Y., Hadaegh, F., Vatankhah, N., Momenan, A.A., Saadat, N., Khalili, D. and Azizi, F. Wrist circumference as a novel predictor of diabetes and prediabetes: results of cross-sectional and 8.8-year follow-up studies. *The Journal of Clinical Endocrinology & Metabolism*, *98*(2):777-784, 2013.
9. Fox, Jeremy. "Average Wrist Size Statistics for Male & Female | Nutritioneering."*Nutritioneering*, www.bodybuildingmealplan.com/average-wrist-size/, 14 Sept. 2022.
10. "Dielectric Properties of Body Tissues: HTML Clients." *Niremf.ifac.cnr.it*, niremf.ifac.cnr.it/tissprop/htmlclie/htmlclie.php.
11. Hartsgrove, G., Kraszewski, A. and Surowiec, A. Simulated biological materials for electromagnetic radiation absorption studies. *Bioelectromagnetics: Journal of the Bioelectromagnetics Society, The Society for Physical Regulation in Biology and Medicine, The European Bioelectromagnetics Association*, *8*(1):29-36, 1987.

12. Mobashsher, A.T. and Abbosh, A.M. Three-dimensional human head phantom with realistic electrical properties and anatomy. *IEEE Antennas and Wireless Propagation Letters*, *13*:1401-1404, 2014.
13. Kobayashi, T., Nojima, T., Yamada, K. and Uebayashi, S. Dry phantom composed of ceramics and its application to SAR estimation. *IEEE transactions on Microwave Theory and Techniques*, *41*(1):136-140, 1993.
14. Mobashsher, A.T. and Abbosh, A.M. Artificial human phantoms: Human proxy in testing microwave apparatuses that have electromagnetic interaction with the human body. *IEEE Microwave Magazine*, *16*(6):42-62, 2015.
15. Gabriel, C. Tissue equivalent material for hand phantoms. *Physics in Medicine & Biology*, *52*(14):4205, 2007.
16. Garrett, J. and Fear, E. Stable and flexible materials to mimic the dielectric properties of human soft tissues. *IEEE Antennas and Wireless Propagation Letters*, *13*:599-602, 2014.
17. Nikitin, P.V., Rao, K.V.S. and Lazar, S. An overview of near field UHF RFID. In *2007 IEEE international conference on RFID*, pages: 167-174, March 2007, IEEE.
18. Balanis, C.A. *Advanced engineering electromagnetics*. John Wiley & Sons, 2012.
19. Balanis, C.A. *Antenna theory: analysis and design*. John wiley & sons, 2016.
20. Ur-Rehman, M., Abbasi, Q.H., Akram, M. and Parini, C. Design of band-notched ultra wideband antenna for indoor and wearable wireless communications. *IET Microwaves, Antennas & Propagation*, *9*(3):243-251, 2015.
21. Khan, Q.U., Fazal, D. and bin Ihsan, M. Use of slots to improve performance of patch in terms of gain and sidelobes reduction. *IEEE Antennas and Wireless Propagation Letters*, *14*:422-425, 2014.